Journal of Nuclear Medicine, published on March 17, 2022 as doi:10.2967/jnumed.121.263136

The Overlap Index as a means of evaluating early tau-PET signal reliability

Jeyeon Lee[1]*, Brian J. Burkett[1], Hoon-Ki Min[1], Emily S. Lundt[2], Sabrina M. Albertson[2], Hugo Botha[3], Matthew L. Senjem[4], Jeffrey L. Gunter[1], Christopher G. Schwarz[1], David T. Jones[3], David S. Knopman[3], Clifford R. Jack Jr.[1], Ronald C. Petersen[3], and Val J. Lowe[1]

[1]Department of Radiology, [2]Department of Health Sciences Research, [3]Department of Neurology, [4]Department of Information Technology, Mayo Clinic

Correspondence: Jeyeon Lee, Ph.D., Department of Radiology, Mayo Clinic, 200 First Street SW, Rochester, Minnesota, 55905, USA.

E-mail: lee.jeyeon@mayo.edu

Running title: OI method for early tau-PET detection

Word count: 4998 (all inclusive)

Funding

This research was supported by NIH grants, P50 AG016574, R01 NS89757, R01 NS089544, R01 DC10367, R01 AG011378, R01 AG041851, R01 AG034676, R01 AG054449, R01 NS097495, U01 AG006786, R21 NS094489, by the Robert Wood Johnson Foundation, The Elsie and Marvin Dekelboum Family Foundation, the Liston Family Foundation and by the Robert H. and Clarice Smith and Abigail van Buren Alzheimer's Disease Research Program, the Alexander Family Foundation, the GHR Foundation, Foundation Dr. Corinne Schuler and the Mayo Foundation for Medical Education and Research.

ABSTRACT

In tau positron emission tomography (tau-PET), a reliable method to detect early tau accumulation in the brain is crucial. Noise, artifacts, and off-target uptake impede detection of subtle true positive ligand binding. We hypothesize that identifying voxels with stable activity over time can enhance detection of true positive tau. **Methods**: 339 participants in the clinical spectrum ranging from clinically unimpaired to Alzheimer's Disease Dementia underwent ≥2 serial tau-PET scans with flortaucipir. The "overlap index" (OI) method was proposed to detect spatially identical, voxel-wise standardized uptake value ratio (SUVR) elevation when seen sequentially in serial tau-PET scans. The association of OI with tau accumulation, clinical diagnosis, and cognitive findings was evaluated. **Results**: OI showed good dynamic range in the low-SUVR window. Only OI was able to identify subgroups with increasing tau-PET signal in low SUVR meta-ROI groups. OI showed improved association with early clinical disease progression and cognitive scores versus meta-ROI SUVR measures. **Conclusion**: OI was more sensitive to tau signal elevation and longitudinal change than standard ROI measures, suggesting it is a more sensitive method for detecting early, subtle deposition of neurofibrillary tangles.

Keywords

AV-1451; Flortaucipir; Tau PET; Variability; early detection.

INTRODUCTION

Alzheimer's disease (AD) is a heterogeneous neurodegenerative disorder characterized by abnormal extracellular amyloid-β (Aβ) plaques and intracellular tau neurofibrillary tangles (NFT)(*1*). The amyloid cascade hypothesis suggests Aβ as the primary cause of tau NFT formation and ultimately neuronal loss(*2*). However, it has also been suggested that the aggregation of pathologic Aβ and tau might be independent etiologies of AD pathology(*3*). Studies have found a clear association between AD severity and increased tau with positron emission tomography (PET)(*4*) and that tau-PET is a better predictor of AD dementia (ADD) than amyloid status(*1,5*). Tau is therefore an attractive target as a biomarker for ADD diagnosis and treatment outcome measure.

Tau-PET uptake patterns have been associated with Braak NFT staging(*6*) and ADD severity(*7,8*). Tau-PET signal is associated with aging(*4*) and with reduced glucose metabolism(*7*) and can distinguish among clinical phenotypes(*7*). Longitudinal amyloid PET has been studied extensively, tracking participants for over a decade(*9*). Longitudinal tau-PET studies are in the initial stage of optimization(*10-12*). Global increases in tau accumulation have been reported, rather than the region-specific sequence that would be expected from the neuropathology literature(*4,10*). More longitudinal tau studies are needed to better understand AD pathogenesis.

Longitudinal tau-PET reliability is limited by inter-scan variability. The standardized-uptake-value-ratio (SUVR) is the most common quantitative measure of

radiotracer uptake. SUVR annual change in longitudinal studies has been relatively small compared to group averages(*10-12*). Annual AV-1451 (Flortaucipir) tau-PET SUVR change in patients with amyloid-positivity and cognitive impairment was around 0.05 SUVR(*10-12*), about 3% of the average cross-sectional SUVR (=1.64) for the group(*4*). The annual increase was similar to the test-retest variability of AV-1451 with 48-hour to 4-week intervals (SUVR changes of up to 0.05)(*13*). Moreover, for cognitively unimpaired (CU) subjects with amyloid positivity, possibly the earliest stage of AD, the mean annual SUVR change has been estimated at 0.006(*10*).

It is therefore important to understand the nature of the variability in serial tau-PET scans when neuropathologically-related PET signal changes may be small. Variability is especially problematic in the early stages of tau pathology in which the rate of NFT accumulation is slow and thus difficult to discern relative to the range of random fluctuation noise in tau-PET imaging. To address this problem, we developed a measure of consistency across serial scans called the “overlap index” (OI) based on the hypothesis that random noise/artifacts are unlikely to be repeated over serial scans and voxels with stable signal over time more likely represent true NFT-related binding. We evaluated the ability of OI to measure early, subtle tau-PET signal change, compared to standard region-of-interest (ROI)-based measure, and evaluated for correlation with changes in clinical status.

MATERIALS AND METHODS

Participants

Eligible participants (n=339) selected from the Mayo Clinic Study of Aging or the Alzheimer's Disease Research Center had ≥2 serial flortaucipir tau-PET scans with MRI, corresponding to 850 tau-PET scans in total(Supplementary Table1)(*10*). Studies were approved by the Mayo Clinic and Olmsted Medical Center Institutional Review Boards. Written informed consent was obtained. Enrolled participants are determined to be clinically normal or cognitively impaired by a consensus panel consisting of study coordinators, neuropsychologists, and behavioral neurologists. Methods for defining CU, mild cognitive impairment (MCI), and dementia in both studies conform to standards in the field(*14-16*). To examine the generalizability of the OI, we also included the longitudinal tau-PET data (n=235,Supplementary Table2-3) from the Alzheimer's Disease Neuroimaging initiative (ADNI) database (adni.loni.usc.edu).

Neuroimaging Methods

Tau-PET imaging was performed with F18-flortaucipir and amyloid-PET with Pittsburgh compound B (PiB) as reported previously(*17*) (see Supplementary Methods(*18-25*)). Tau- and amyloid-PET SUVR were normalized to the median uptake in the cerebellar crus. The regional tau-PET SUVRs were calculated by measuring median uptake in each ROI, excluding any voxels segmented as cerebrospinal fluid. A meta-ROI for tau-PET included the amygdala, entorhinal cortex (ERC), fusiform, parahippocampal and inferior temporal and middle temporal gyri(*10,24*). The tau-PET meta-ROI SUVR was calculated as an average of the median SUVR in each region.

Global cortical amyloid-PET SUVR was computed as a voxel-number weighted average of median uptake across a set of ROIs including the prefrontal, orbitofrontal, parietal, temporal, anterior and posterior cingulate, and precuneus ROIs(*24*). An SUVR>1.29 threshold denoted abnormal tau-PET scans(*6*). The threshold used to define abnormal PiB-PET was SUVR=1.42(*24*). Meta-ROI ΔSUVR was calculated as an annualized difference between the baseline SUVR from the follow-up SUVR.

Overlap Index Calculation

OI represents the voxel-wise SUVR elevation consistently present on two serial scans(Fig.1). First, we selected the ROI(or meta-ROI) to be evaluated in the calculation. An intensity threshold (SUVR=1.4) -selected from preliminary experimental tests(Supplementary Fig.1)- was applied to each voxel in the ROI(s). Voxels that survived the intensity threshold were binarized (0/1) as masks (M_b and M_f). Clusters with fewer than 20 contiguous voxels (18-connectivity criterion) were excluded. The spatial overlap between masks ($N_{overlap}$) was calculated by counting the number of voxels with an intensity of 1 after multiplying the two masks. OI was calculated by dividing $N_{overlap}$ by the number of voxels where the value is 1 in the M_b (N_b).

$$Overlap\ index\ (OI) = \frac{N_{overlap}}{N_b}$$

Values of 0 indicate no overlap between scans; conversely, values approaching 1 indicate consistent elevation of voxels in the follow-up scan.

Unlike standard indices that calculate overlap (*e.g.*, Dice coefficient or Jaccard index), OI is asymmetrically normalized with to the value in only the first scan. Hence,

OI quantifies the extent to which the high-intensity voxels of the first scan are spatially preserved in the second scan. Biologically, the increased topographic extent of tau uptake over time is usually expected. Therefore, we assumed that the index calculated by a standard symmetric measure (*i.e.*, denominator is a union of both scan) could be less sensitive to the detection of early tau where only a small amount of NFT would exist. An overlap size (OS) quantifying a ratio of the overlap area to the size of the total ROI(s), was also defined as following:

$$Overlap\ size\ (OS) = \frac{N_{overlap}}{N_{ROI}}$$

N_{ROI} is the number of voxels of ROI(s) included for the analysis. The OI and OS were calculated for each serial scan pair.

Statistical Analysis

To test for significant group differences in OI and SUVR, we ran non-parametric Kruskal-Wallis tests, followed by *post-hoc* Dunn's multiple comparison test. Non-parametric tests were applied as they do not require the data to be normally distributed. To address different stages of the typical Alzheimer's continuum, we separated the CU participants using the amyloid positivity: CU individuals with normal amyloid-PET (CUA-, i.e. not in the Alzheimer's continuum) and CU individuals with abnormal amyloid-PET (CUA+, i.e. early in the Alzheimer's continuum). Then, the clinical change seen in participants at the time points of the serial scans were grouped as CUA-toCUA-, CUA-toCUA+, CUA+toCUA+ CUtoMCI/AD, MCItoMCI, MCItoAD, and ADtoAD. For more details, please refer to the supplementary data.

RESULTS

Association of OI with SUVR in Single ROI

Scatter plots of voxel intensity within 3D space for a specific ROI demonstrate both low and high-OI examples(Fig.2). For low-OI(Fig.2A), inconsistent voxel signal elevation over serial scans can be seen even when median SUVR of the overall region is above the autopsy tau-PET threshold (SUVR=1.29). The median SUVR fluctuated above and below the threshold in these examples. Conversely, high-OI examples(Fig.2B) show consistent high-intensity voxels over serial scans, with voxels clusters gradually enlarging based on visual assessment even when the median SUVR did not numerically increase. Notably, the median SUVRs of Fig.2B was below threshold. More examples for high-OI can be found in Supplementary Fig.2.

Fig.3 shows the relationship between OI and baseline SUVR for representative ROIs. OI increased exponentially in the low SUVR range and approached 1.0 around SUVR=1.5 (vertical dotted line) for every region. In the SUVR<1.5 range, the SUVR and OI showed a significant linear relationship for all regions ($p<0.005$). The regional distribution of OI and SUVR for both MCI and AD were calculated by anatomic region, ranked and displayed on a 3D-rendered plot(Supplementary Fig.3A-B), corroborating the statistically significant correlation of regional OI and SUVR ($r=0.8489$, Supplementary Fig.3C).

OI Can Characterize Tau Accumulators

Meta-ROI also showed a strong linear correlation with baseline SUVR in the low SUVR range (R^2=0.3806), reaching values near 1.0 around SUVR=1.5(Fig.4A). Most participants (79.65%) had a below-threshold SUVR (<1.5) whereas OI was more evenly distributed(Fig.4A). OI provides a good dynamic range even in this low-SUVR window. This also held true for follow-up scans(Supplementary Fig.4). A relationship between OI and scan interval was tested. High OI values were found even for relatively long scan intervals (>2yrs) in cases where baseline SUVR was high. In contrast, OI was low regardless of the scan interval for low SUVR cases(Supplementary Fig.5). Multivariable linear regression showed that baseline SUVR better explained the OI than the interval(Supplementary table4).

Next, we investigated an association of meta-ROI OI and ΔSUVR. If OI is sensitive to tau burden, the metric would show positive correlation with tau accumulation rate, as an increased extent of tau over time is biologically expected(*10-12*). Supplementary Fig.6A shows pairs of meta-SUVR from two sequential scans for each individual subject. Then, the total cohort was separated into low-OI (OI<0.5) and high-OI (OI>0.5) subgroups(Supplementary Fig.6B-C). Importantly, OI discriminates positive tau accumulation (slope>0) from stable tau. Statistically, a significant positive correlation between OI and ΔSUVR was also demonstrated (R^2=0.1603, p<0.0001;Fig.4B). This significance held true for baseline SUVR>1.5(Supplementary Fig.7A; R^2=0.1566,p<0.0001).

Comparison of baseline meta-SUVR value groups (SUVR<1.29,1.29<SUVR<1.5 and SUVR>1.5) showed increased ΔSUVR with increased baseline values (p=0.001); however, the comparison between SUVR<1.29 and 1.29<SUVR<1.5 did not reach significance (Fig.4C;p=0.46). A significant difference in ΔSUVR was detected between low-OI and high-OI groups within the same SUVR range (Fig.4D;p=0.01 and p=0.006 for SUVR<1.29 and 1.29<SUVR<1.5, respectively). Notably, the average ΔSUVR in the low-OI group was close to zero or even negative (mean=0.002 and -0.048 for SUVR<1.29 and 1.29<SUVR<1.5, respectively), whereas high-OI groups showed a positive tendency in ΔSUVR (mean=0.025, 0.019 and 0.041 for SUVR<1.29, 1.29<SUVR<1.5 and SUVR>1.5, respectively). There was no significant difference among high-OI groups at different SUVR levels. These results imply that the OI can distinguish tau accumulation within meta-SUVR subgroups that cannot be detected by SUVR alone. To test the reliability, we compared the meta-ROI OI from the first and second scans to the second and third scans, when three or more time points were available. The OI of 1-2 and the OI of 2-3 were highly correlated (r=0.8902) meaning OI is consistent over time(Supplementary Fig.7B).

Meta-ROI OI Relationship to Demographic Data

A pairwise comparison with CUA-toCUA- as the control group demonstrated that OI can detect significant differences from the other subgroups including the smallest degree of clinical change, CUA-toCUA+(Fig.5). Baseline SUVR, baseline $SUVR_{pvc}$, and ΔSUVR from meta-ROI also showed significant differences from the MCI groups,

however no significant difference was seen in comparison with the earlier disease progression groups such as CUA-toCUA+, CUA+toCUA+ and CUtoMCI/AD.

The relationship of cognitive scores with meta-ROI OI and SUVR was also investigated. We found that the meta-ROI OI and meta-SUVR had a significant linear relationship with the cognitive scores(Supplementary Fig.8A-B;linear regression, $p<0.005$). However, the cognitive scores associated more strongly with OI than the SUVR for the global, language, and visuospatial domain (for OI, R^2=0.2209, 0.2054 and 0.1288 for global, language, and visuospatial domain, respectively and for meta-SUVR, R^2=0.1731, 0.1275 and 0.0667 for global, language and visuospatial domain, respectively). For the memory and attention domain, both showed a similar result (for OI, R^2=0.1859 and 0.1337 for memory and attention domain, respectively and for follow-up meta-SUVR, R^2=0.1810 and 0.1422 for memory and attention domain, respectively)

To evaluate the generalizability of OI metric, we tested OI in the ADNI dataset. This validated many of the results seen in the Mayo cohort. For meta-ROI, OI reached approached 1.0 around SUVR=1.5(Fig.6A). In addition, meta-ROI OI-based grouping was able to discriminate the positive tau accumulator within the same SUVR range(Fig.6C; $p<0.001$ for SUVR<1.29 and $p=0.02$ for 1.29<SUVR<1.5) while meta-SUVR subgroups separated by baseline SUVR did not reach statistical significance (Fig.6B). In the disease progression assessment, the patterns were overall similar to those of the Mayo dataset, where CUA+toCUA+ and CUtoMCI/AD groups showed significant differences of OI compared to CUA-toCUA- ($p<0.001$ and $p=0.0476$ for

CUA+toCUA+ and CUtoMCI/AD, respectively;Fig.6D). However, fewer significant differences were found in SUVR measurements between groups(Fig.6D).

DISCUSSION

In this study, we proposed OI as a means for early detection of tau-PET bindings by evaluating consistency of serial tau-PET scans and tested the ability of OI to identify subtle, but true positive tau binding in serial scans. Participants with high-OI had a larger serial SUVR change than participants with low-OI, a finding which notably was also seen with participants below the tau cut-off (SUVR<1.29). When compared to ROI-based SUVR measurements, OI alone had a significant association with early disease progression.

Although SUVR and OI showed a significant linear correlation, OI showed better dynamic range in the low-SUVR window. It may be that the typical ROI-based measures that calculate the median SUVR all voxels are less sensitive to the early development of NFT because the local tau-PET signal can be diluted in the process of obtaining the median of the entire ROI(s)(*6*). In contrast to the ROI method, OI quantifies the spatial consistency only in those voxels with an elevated tau-PET signal. This characteristic of OI is independent of the size of the tau cluster, thus allowing better characterization of small areas of signal elevation in the low SUVR range in which NFT volume is relatively small. In this respect, OI can better detect early stages of tau pathology than the typical ROI-based measurements. In the high SUVR range, this provides less added value because consistency is high when tau is abundant(Supplementary Fig.9). Because AD

is a chronic and progressive disease, early detection before devastating symptoms begin is critically important. Tau-PET is in general a promising biomarker, more closely associated with disease severity than other imaging biomarkers;(*26*) however, inter-scan random variability which does not represent true tau pathology presents a significant hurdle(*13,27*). A recent autopsy study reported that ROI methods be insufficient to detect subtle tau-PET signals in early tau deposition(*6*), probably reflecting diminished signal-to-noise when a small volume of true radiotracer binding is present(*28*). Our results suggest that OI may overcome this limitation and be complementary to typical ROI measures for interpreting the early tau-PET signal.

OI will likely be also useful in distinguishing true tau accumulation from random variability in longitudinal studies. Our results showed that OI can characterize the participants who will accumulate tau amongst those in the low-SUVR and mid-SUVR groups better than meta-ROI. As described earlier, as an increased extent of NFT over time is biologically expected(*10-12*), OI which is sensitive to subtle tau burden may better identify subjects with true accumulation that was hidden by ROI SUVR washout or random variability. Clearly, there is a wide standard deviation in the high meta-ROI group with some participants showing negative change. This phenomenon of negative change was also observed in previous longitudinal studies reporting some individuals with high baseline SUVR and negative SUVR changes(*10-12*). The reasons for these negative SUVR changes are not yet well understood. CSF phosphorylated tau level could decrease in the late AD(*29*) accounting for the negative change. Noise or partial volume effects due to tau aggregation-driven local atrophy may contribute(*30,31*).

Further optimization of OI methods to target the high meta-ROI group is an aim of our ongoing work.

OI was highest in the inferior, middle, and medial temporal lobes including the ERC, and amygdala, areas of elevated tau PET activity described in the literature(*8,32*). While nonspecific binding related to AV1451 is not well understood in longitudinal data, a possible limitation is that OI may be vulnerable to suprathreshold off-target binding when it consistently occurs in serial scans. For example, the hippocampal OI may be vulnerable to choroid plexus(Supplementary Fig.10). To minimize this, typical non-specific binding areas such as basal ganglia and choroid plexus are excluded from meta-ROI analysis. Four cases of non-specific binding in meninges were observed which only affected the OI measurement when meninges had repeated strong signal in the meta-ROI (Supplementary Fig.11). Future work is needed to characterize the effects of off target binding on the SUVR and OI.

The difference between OI and SUVR regarding cognitive findings is marginal. This is not unexpected given that our sample population is mixed and comprised of those without significant cognitive impairment (i.e., CU; ~50% of sample), MCI, or early AD (28% of sample) some of whom have little or no cognitive impairment. Our plans are to expand the OI analysis to larger groups of subjects with cognitive impairment to better define clinically utility.

The statistical significance between early preclinical groups (i.e., CUA-toCUA- vs. CUA-toCUA+) was only demonstrated in the Mayo cohort. Notably, the mean OI values of CUA-toCUA+ group were not different between the cohorts ($p=0.9652$, mean OI=0.3573 and 0.3558 for Mayo and ADNI, respectively), but the CUA-toCUA- group showed significantly different mean OI between the cohorts ($p<0.001$, mean OI=0.1832 and 0.3125 for Mayo and ADNI, respectively). One possible explanation is the relatively smaller number of samples in the CUA-toCUA- group from ADNI cohort (97 for Mayo vs. 26 for ADNI). However, the reason for high OI values in the early preclinical groups should be investigated with neuropathology studies in the future.

One limitation of this study is the assumption that voxels with artifactual or false-positive activity would be less likely to show spatial consistency over-time, an assumption that should be validated with post-mortem neuropathologic data of tau deposition. The SUVR is sensitive to perfusion changes; therefore, interscan comparison may be biased when perfusion differs between the two scans. Despite this limitation, OI performs better for early detection of tau-PET signal and disease progression than the ROI-based SUVR measure. Future investigation with simulation studies will be needed to assess the magnitude of the bias of perfusion on OI. The intensity threshold used in this study was determined observationally. The OI calculation is largely dependent on this threshold level and future work is warranted to determine the optimal threshold among different regions and even at voxel level. Although OI can augment sensitivity to early tau-PET uptake, acquiring two separate PET scans is a disadvantage. Using dynamic scans to derive OI from a single imaging session by

splitting the scan into two segments may address this limitation. Future investigation of this possible solution is needed, which will require careful optimization given the slow kinetics of the AV-1451 tracer.

CONCLUSION

By identifying voxels with consistent signal, the OI method could be helpful in measuring early tau-PET signal. This voxel-wise analysis can overcome the limitations of ROI-based measures which had reduced sensitivity to early detection of low levels of tau. The ability of OI to reliably detect true positive binding is likely to have the most impact in the lower SUVR window, reflecting the early stage of neurodegeneration and early tau NFT pathology prior to cognitive decline. Combining the OI method with other methods which minimize inter-scan variability (partial volume correction and optimized reference) may synergistically improve interpretations of longitudinal change in the tau-PET signal.

ACKNOWLEDGMENTS

The authors are grateful to Penelope Duffy, Ph.D. for editorial contributions and review.

DISCLOSURE

Mr. Senjem has owned stocks and/or options in the following medical-related companies: Align Technology, Inovio Biomedical, Johnson & Johnson, Mesa Laboratories, Nvidia, LHC Group, Natus Medical Incorporated, Varex Imaging Corporation, CRISPR Therapeutics, Gilead Sciences, Ionis Pharmaceuticals, and Medtronic. Dr. Gunter reports an abandoned provisional patent for face replacement in MR imaging unrelated to the current publication. Dr. Schwarz has given lectures sponsored by Karolinska Institute unrelated to the current publication. Dr. Knopman served on a data safety monitoring board for the DIAN study, serves on a data safety monitoring board for a Biogen tau therapeutic, and is a site investigator in the Biogen aducanumab trials, an investigator in clinical trials sponsored by Lilly Pharmaceuticals and USC, and a consultant for Samus Therapeutics, Third Rock, Roche and Alzeca Biosciences but receives no personal compensation. Dr. Jack serves on an independent data monitoring board for F. Hoffmann-La Roche, has consulted and spoken for Eisai, and has consulted for Biogen but receives no personal compensation from any commercial entity. Dr. Petersen receives research support from GHR Foundation, has received royalties from Oxford University Press, is a member of a data safety monitoring board for Genentech, and is a consultant for Roche, Merck, Biogen, and Eisai. Dr. Lowe receives research support from GE Healthcare, Siemens Molecular Imaging, and AVID Radiopharmaceuticals, and consults for Bayer Schering, Piramal Life Sciences, Life Molecular Imaging, Eisai, AVID Radiopharmaceuticals, and Merck. No other potential conflicts of interest relevant to this article exist.

KEY POINTS

Question: Is identifying voxels with stable signal over time a more sensitive method for detecting early, subtle development of neurofibrillary tangles?

Pertinent Findings: Only OI was able to identify subgroups with increasing tau-PET signal in low SUVR meta-ROI groups. OI showed improved association with early disease progression and cognitive scores vs. meta-ROI SUVR measures.

Implications for Patient Care: Our findings demonstrate that the proposed method could be helpful in detecting tau signal elevation and longitudinal changes than standard ROI measures, suggesting it is less vulnerable to random variability and more sensitive to early, subtle ligand binding.

Graphical abstract

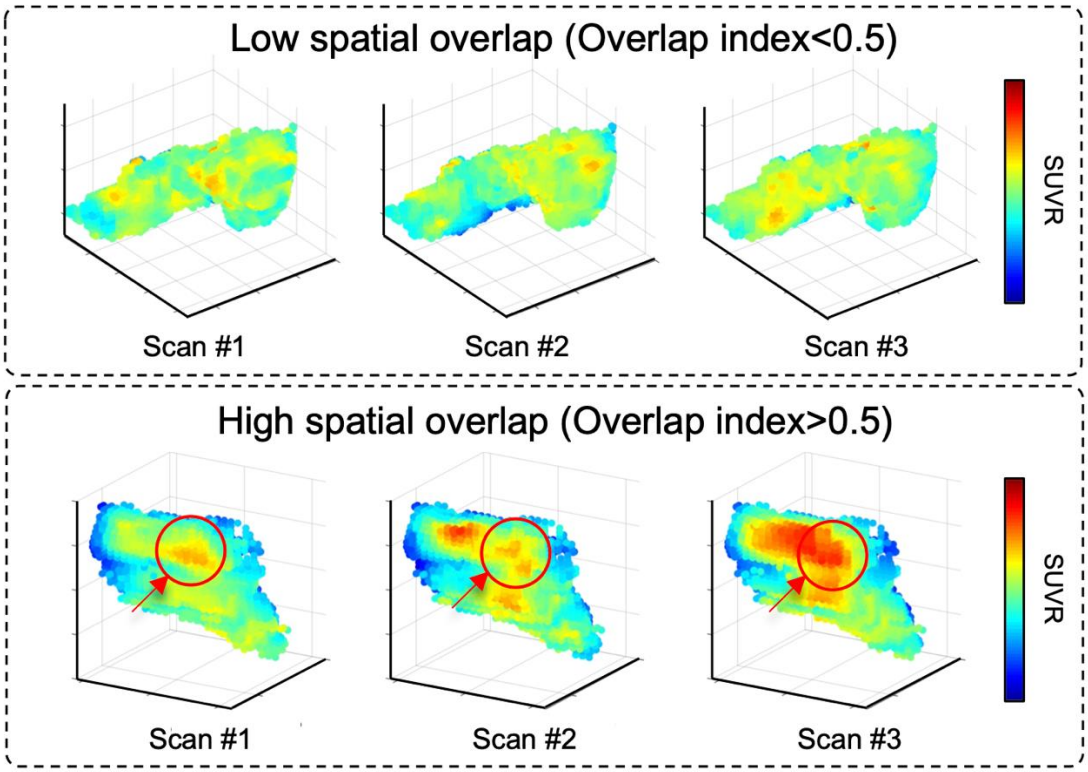

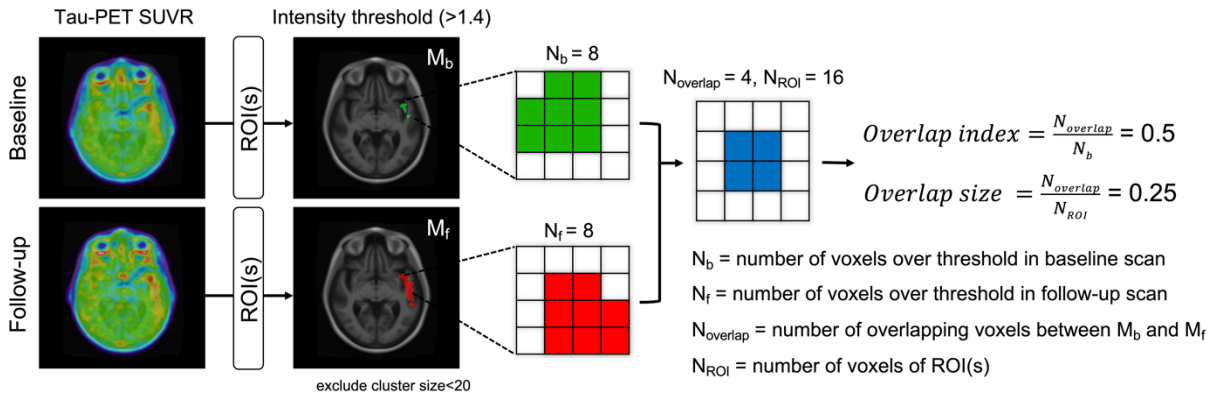

Figure1. Overlap index (OI) calculation. OI was designed to identify voxels with stable high activity over time using two consecutive tau-PET scans.

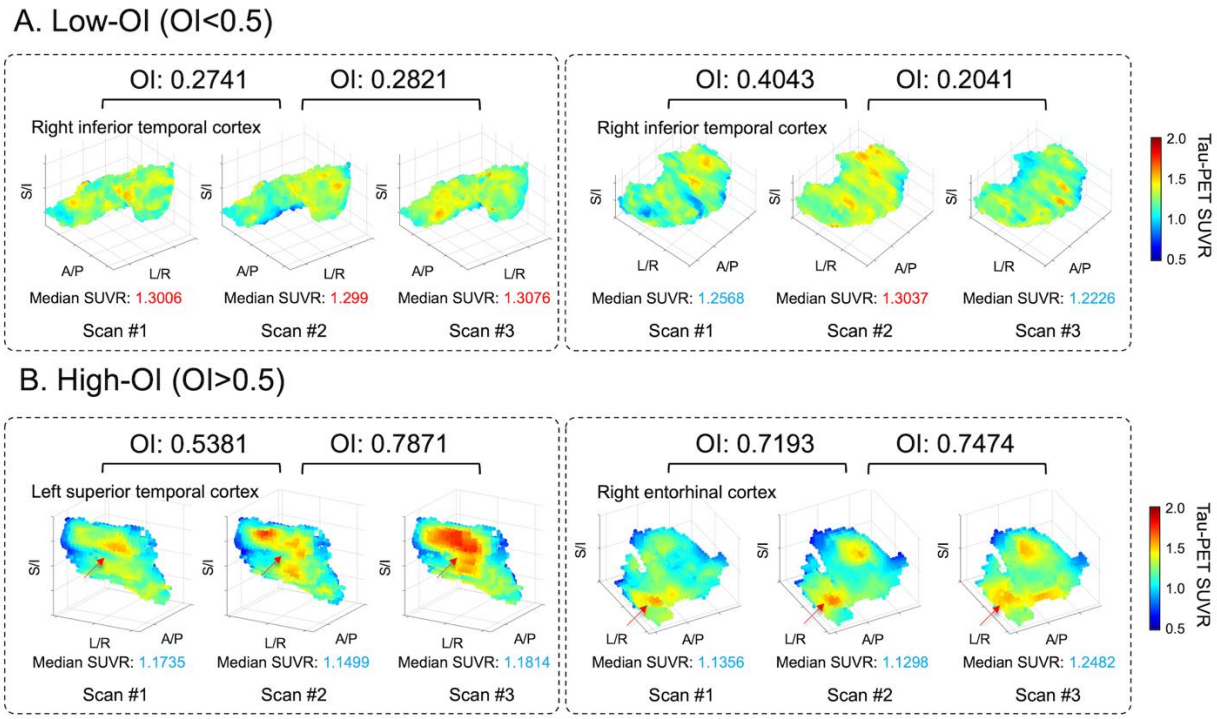

Figure 2. Examples for low-OI and high-OI. Three consecutive 3D scatter plots are displayed in each box for four different examples, representing the tau-PET SUVR of each voxel in each scan from an individual subject. (A) shows low-OI and (B) shows high-OI cases. Below each rendering, the median SUVR represents a median value for all voxels in each region. The colorbar indicates the intensity of each voxel. Font color of median SUVR is red when >1.29 and blue when <1.29. Red arrows in B indicate the regions showing spatial consistency. Various anatomic regions are plotted and labeled in each panel.

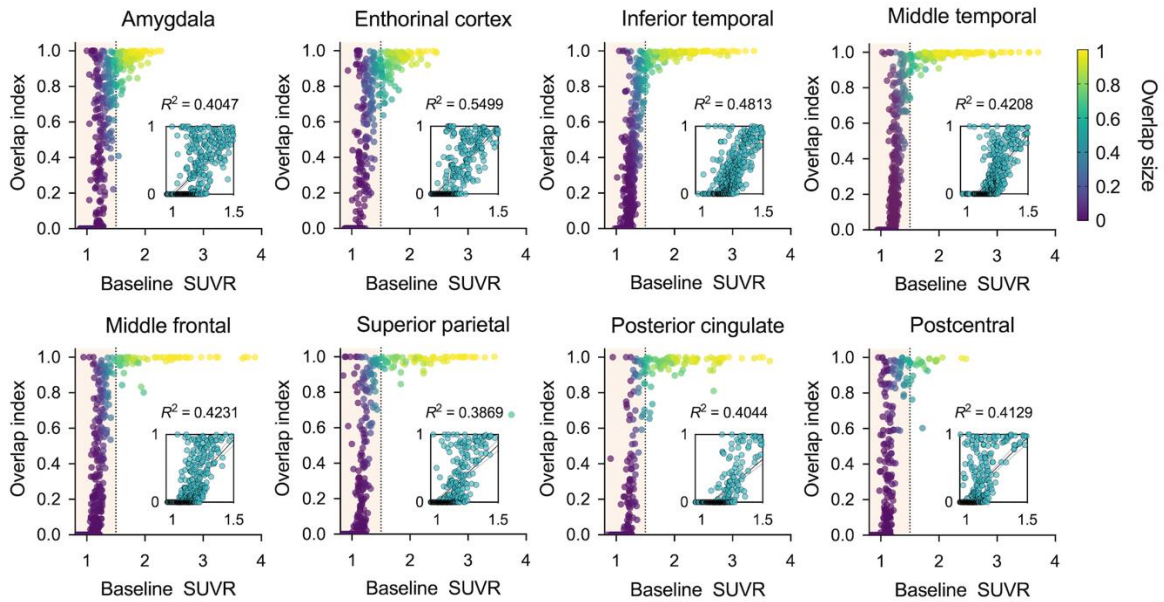

Figure 3. Relationship between OI and baseline SUVR in single ROI. Bilateral ROIs were included in the calculations. A small panel inside the figure illustrates an enlarged view of the lower SUVR range (from 0.9 to 1.5).

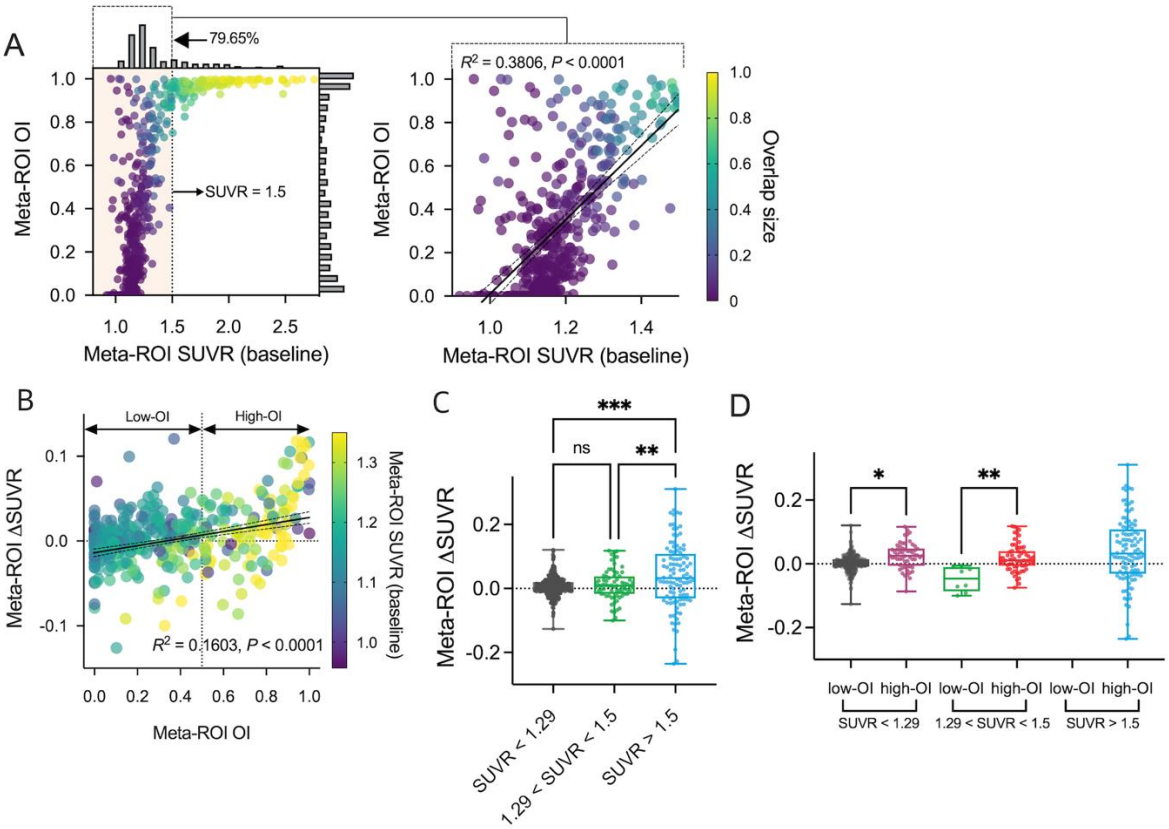

Figure 4. Relationship between meta-ROI OI and meta-ROI SUVR. (A) A scatterplot (left) of baseline SUVR and OI for meta-ROI. Histograms are displayed along SUVR and OI axis, respectively. The low SUVR range (<1.5) was magnified in a separate scatterplot (right) with linear regression (solid black line) and 95% confidence band (dotted black lines). (B) Scatterplot of meta-ROI OI and ΔSUVR with regression. (C) Comparison of ΔSUVR between SUVR based subgroups. (D) The SUVR based subgroups in C were further separated into low-OI and high-OI categories. *p<0.05, **p<0.05, ***p<0.005, *post-hoc* Dunn's tests.

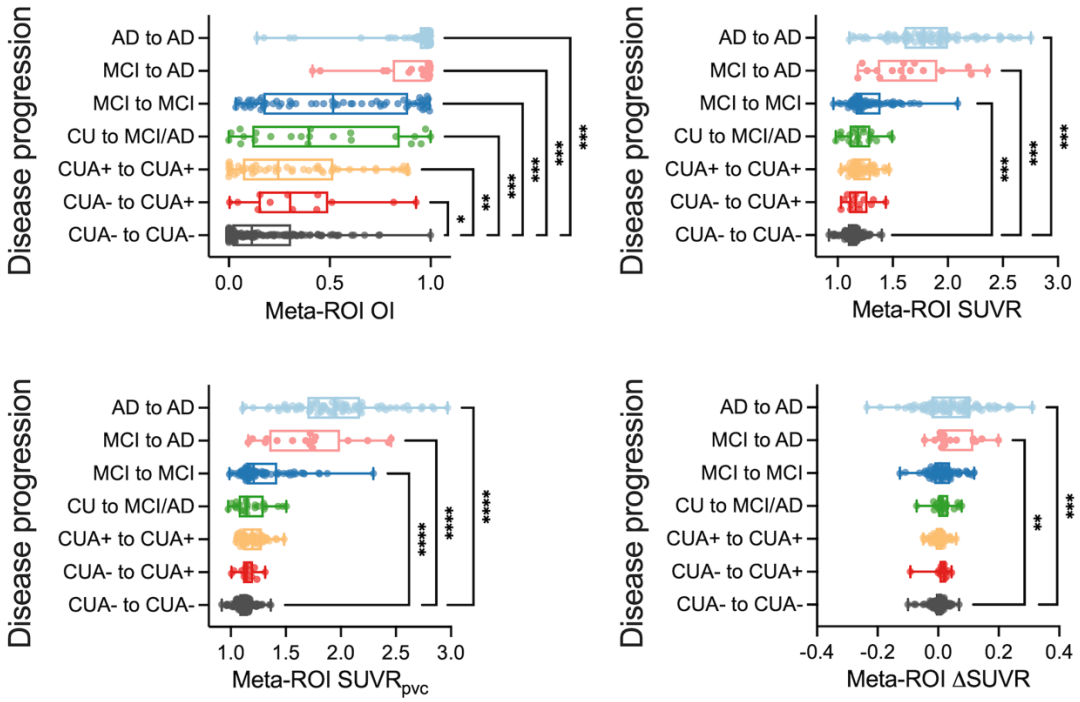

Figure 5. Association of overlap index with disease progression. (A) Tau-PET variables in different clinical groups. OI, baseline SUVR, baseline $SUVR_{pvc}$, and ΔSUVR from meta-ROI of CUA-toCUA- were compared with those of other groups. *p<0.05, **p<0.05, ***p<0.005, *post-hoc* Dunn's tests.

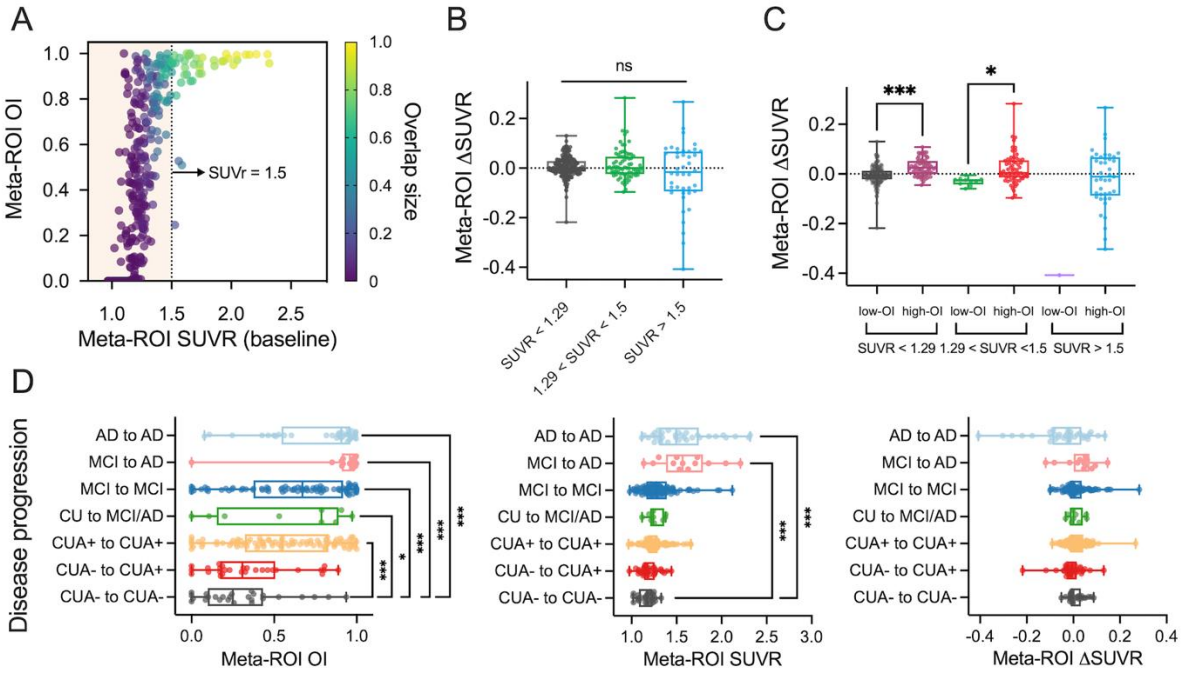

Figure 6. Result for ADNI cohort. (A) Scatterplot of baseline SUVR and OI for meta-ROI. (B) Comparison of ΔSUVR between SUVR based subgroups. (C) The SUVR based subgroups in B were further separated into low-OI and high-OI categories. (D) OI, baseline SUVR, and ΔSUVR from meta-ROI of CUA-toCUA- were compared with those of other groups. *p<0.05, **p<0.05, ***p<0.005, *post hoc* Dunn's tests.

References

1. Nelson PT, Alafuzoff I, Bigio EH, et al. Correlation of Alzheimer disease neuropathologic changes with cognitive status: a review of the literature. *J Neuropathol Exp Neurol.* 2012;71:362-381.

2. Hardy J, Selkoe DJ. The amyloid hypothesis of Alzheimer's disease: progress and problems on the road to therapeutics. *science.* 2002;297:353-356.

3. Wisniewski T, Goñi F. Immunotherapy for Alzheimer's disease. *Biochem Pharmacol.* 2014;88:499-507.

4. Lowe VJ, Wiste HJ, Senjem ML, et al. Widespread brain tau and its association with ageing, Braak stage and Alzheimer's dementia. *Brain.* 2018;141:271-287.

5. Ossenkoppele R, Smith R, Ohlsson T, et al. Associations between tau, Aβ, and cortical thickness with cognition in Alzheimer disease. *Neurology.* 2019;92:e601-e612.

6. Lowe VJ, Lundt ES, Albertson SM, et al. Tau-positron emission tomography correlates with neuropathology findings. *Alzheimers Dement.* 2019;16:561-571.

7. Ossenkoppele R, Schonhaut DR, Schöll M, et al. Tau PET patterns mirror clinical and neuroanatomical variability in Alzheimer's disease. *Brain.* 2016;139:1551-1567.

8. Johnson KA, Schultz A, Betensky RA, et al. Tau positron emission tomographic imaging in aging and early A lzheimer disease. *Ann Neurol.* 2016;79:110-119.

9. Jack CR, Wiste HJ, Lesnick TG, et al. Brain β-amyloid load approaches a plateau. *Neurology.* 2013;80:890-896.

10. Jack Jr CR, Wiste HJ, Schwarz CG, et al. Longitudinal tau PET in ageing and Alzheimer's disease. *Brain.* 2018;141:1517-1528.

11. Cho H, Choi JY, Lee HS, et al. Progressive tau accumulation in Alzheimer disease: 2-year follow-up study. *J Nucl Med.* 2019;60:1611-1621.

12. Pontecorvo MJ, Devous MD, Kennedy I, et al. A multicentre longitudinal study of flortaucipir (18F) in normal ageing, mild cognitive impairment and Alzheimer's disease dementia. *Brain.* 2019;142:1723-1735.

13. Devous MD, Joshi AD, Navitsky M, et al. Test–retest reproducibility for the tau PET imaging agent Flortaucipir F 18. *J Nucl Med.* 2018;59:937-943.

14. Albert MS, DeKosky ST, Dickson D, et al. The diagnosis of mild cognitive impairment due to Alzheimer's disease: recommendations from the National Institute on Aging-Alzheimer's Association workgroups on diagnostic guidelines for Alzheimer's disease. *Alzheimers Dement.* 2011;7:270-279.

15. McKhann GM, Knopman DS, Chertkow H, et al. The diagnosis of dementia due to Alzheimer’s disease: Recommendations from the National Institute on Aging-Alzheimer’s Association workgroups on diagnostic guidelines for Alzheimer's disease. *Alzheimers Dement.* 2011;7:263-269.

16. Petersen RC. Mild cognitive impairment as a diagnostic entity. *J Intern Med.* 2004;256:183-194.

17. Schwarz CG, Gunter JL, Lowe VJ, et al. A comparison of partial volume correction techniques for measuring change in serial amyloid PET SUVR. *J Alzheimers Dis.* 2019;67:181-195.

18. Joshi A, Koeppe RA, Fessler JA. Reducing between scanner differences in multi-center PET studies. *Neuroimage.* 2009;46:154-159.

19. Schwarz CG, Wiste HJ, Gunter JL, et al. Variability in MRI and PET measurements introduced by change in MRI vendor. *Alzheimers Dement.* 2019;15:P104-P105.

20. Tzourio-Mazoyer N, Landeau B, Papathanassiou D, et al. Automated anatomical labeling of activations in SPM using a macroscopic anatomical parcellation of the MNI MRI single-subject brain. *Neuroimage.* 2002;15:273-289.

21. Vemuri P, Whitwell JL, Kantarci K, et al. Antemortem MRI based STructural Abnormality iNDex (STAND)-scores correlate with postmortem Braak neurofibrillary tangle stage. *Neuroimage.* 2008;42:559-567.

22. Ashburner J, Friston KJ. Unified segmentation. *Neuroimage.* 2005;26:839-851.

23. Vemuri P, Senjem ML, Gunter JL, et al. Accelerated vs. unaccelerated serial MRI based TBM-SyN measurements for clinical trials in Alzheimer's disease. *Neuroimage.* 2015;113:61-69.

24. Jack Jr CR, Wiste HJ, Weigand SD, et al. Defining imaging biomarker cut points for brain aging and Alzheimer's disease. *Alzheimers Dement.* 2017;13:205-216.

25. Meltzer CC, Leal JP, Mayberg HS, Wagner Jr HN, Frost JJ. Correction of PET data for partial volume effects in human cerebral cortex by MR imaging. *J Comput Assist Tomogr.* 1990;14:561-570.

26. Villemagne VL, Fodero-Tavoletti MT, Masters CL, Rowe CC. Tau imaging: early progress and future directions. *The Lancet Neurology.* 2015;14:114-124.

27. Timmers T, Ossenkoppele R, Visser D, et al. Test–retest repeatability of [18F] Flortaucipir PET in Alzheimer's disease and cognitively normal individuals. *Journal of Cerebral Blood Flow & Metabolism.* 2020;40:2464-2474.

28. Barthel H. First Tau PET Tracer Approved: Toward Accurate In Vivo Diagnosis of Alzheimer Disease. *Journal of Nuclear Medicine.* 2020;61:1409-1410.

29. Fagan AM, Xiong C, Jasielec MS, et al. Longitudinal change in CSF biomarkers in autosomal-dominant Alzheimer's disease. *Sci Transl Med.* 2014;6:226ra230-226ra230.

30. Sepulcre J, Schultz AP, Sabuncu M, et al. In vivo tau, amyloid, and gray matter profiles in the aging brain. *J Neurosci.* 2016;36:7364-7374.

31. Iaccarino L, Tammewar G, Ayakta N, et al. Local and distant relationships between amyloid, tau and neurodegeneration in Alzheimer's Disease. *Neuroimage Clin.* 2018;17:452-464.

32. Mattsson N, Insel PS, Donohue M, et al. Predicting diagnosis and cognition with 18F-AV-1451 tau PET and structural MRI in Alzheimer's disease. *Alzheimers Dement.* 2019;15:570-580.

Supplemental Data

Neuroimaging methods

T1-weighted MRI was acquired using 3T scanners manufactured by General Electric (GE) and Siemens using a 3D Sagittal Magnetization-Prepared Rapid Acquisition Gradient Recalled Echo (MPRAGE) sequence (number of scans=544 and 306 for GE and Siemens, respectively). During the analysis, two scans were excluded because MRI data was unusable due to motion. Tau-PET and amyloid PET scans were acquired using the PET/CT scanner by GE and Siemens operating in 3D mode (number of scans=817 and 33, for GE and Siemens, respectively for tau-PET; number of scans=782 and 31, for GE and Siemens, respectively for amyloid-PET). To harmonize the inter-scan difference, for PET scanners, different filters were applied to each during reconstruction in order to harmonize resolution according to the method of Joshi et al (*1*). For MRI scanners, we have previously shown that the effects on PET quantification are negligible (*2*). A CT scan was obtained for attenuation correction. For tau-PET, an intravenous bolus injection of ~370 MBq (range 333–407 MBq) F18-flortaucipir was administered, and PET/CT imaging was performed with a 20-minute PET acquisition of four 5-min dynamic frames, 80-100 minutes after injection. Amyloid PET imaging was performed using Pittsburgh compound B (PiB) and consisted of four 5-min dynamic frames, 40–60 min after injection of 628 MBq (range 385–723 MBq) of 11C-PiB. The mean and standard deviation of specific activity for the entire period that the images were acquired was 2.58 (±0.32) Ci/μmol and 3.44 (±0.78) Ci/μmol for PiB and AV1451, respectively. An iterative reconstruction algorithm was applied. Emission data were reconstructed into a 256×256 matrix with a 30-cm field of view (in-plane pixel size = 1.0

mm). Standard corrections for attenuation, scatter, random coincidences and decay were applied as well as a 5 mm Gaussian post-reconstruction filter. The images from the four dynamic frames were averaged to create a single static image.

The static tau-PET image volumes of each participant were rigidly co-registered to the corresponding T1-weighted MRI using 6-degree-of-freedom registration ("spm_coreg") in SPM5. The automated anatomic labeling (AAL) atlas (*3*) was normalized to the custom template (*4*) using the unified segmentation method in SPM5 giving a set of labels corresponding to the custom template space. SPM5 unified segmentation (*5*) with a custom elderly template generated from 200 AD and 200 controls and tissue priors (*4*) was used to segment the MRI into GM, WM, CSF, and to warp the atlas labels from template space to subject space. Within each subject, SPM5 co-registration was performed on the longitudinal series of MRI images to align to the mean across all images, thus forming a new mean image, and repeated until convergence (*6*). SUVR images were normalized to the uptake in the cerebellar crus (*7*). For each timepoint, the tau-PET images were resampled into the space of the mean MPRAGE. The regional SUVRs were calculated by measuring median uptake in each ROI, excluding any voxels segmented as cerebrospinal fluid. A meta-ROI for tau-PET included the amygdala, entorhinal cortex (ERC), fusiform, parahippocampal and inferior temporal and middle temporal gyri (*8,9*). The tau-PET meta-ROI SUVR was calculated as an average of the median SUVR in each region. We did not use a voxel-number weighted average for the meta-ROI SUVR calculation because the weighted average might penalize small ROI values such as for the entorhinal cortex or amygdala,

anatomic regions of known early NFT accumulation. Global cortical amyloid PET SUVR was computed as a voxel-number weighted average of median SUVR in each meta-ROI region including the prefrontal, orbitofrontal, parietal, temporal, anterior and posterior cingulate, and precuneus ROIs (*9*). The threshold used to define abnormal PiB PET was SUVR=1.42 (*9*). All analysis was performed using non-partial volume corrected (PVC) PET images. For comparison with non-PVC images, tau-PET with PVC was evaluated. For the PVC, each PET image voxel was divided by the value in the tissue mask to generate a PVC image (*10*) and an unsmoothed binary MRI grey matter mask applied to yield a grey matter sharpened PET image.

Statistical tests

The association of regional OI and regional SUVR from the total cohort was assessed with Pearson's correlation to evaluate the topographical relationship of the two measurements. An association of OI with SUVR in the lower SUVR range (<1.5) was tested using linear regression. Meta-ROI ΔSUVR for each individual was calculated by subtracting the baseline SUVR from the follow-up SUVR and dividing by the time difference in years. To investigate the association of OI with meta-ROI ΔSUVR, the total cohort was separated into three sub-groups (SUVR<1.29, 1.29<SUVR<1.5 and SUVR>1.5) of baseline meta-ROI SUVR, further separated into low-OI (OI<0.5) and high-OI (OI>0.5) group based on meta-ROI OI value. The difference of meta-ROI ΔSUVR between groups was tested by *post-hoc* Dunn's multiple comparison test after non-parametric Kruskal-Wallis tests. To address different stages of the typical Alzheimer's continuum, we separated the CU participants using the amyloid positivity: CU individuals with normal amyloid PET (CUA-, i.e. not in the Alzheimer's continuum)

71 and CU individuals with abnormal amyloid PET (CUA+, i.e. early in the Alzheimer's
72 continuum). Then, the clinical change seen in participants at the time points of the serial
73 scans were grouped as CUA-toCUA-, CUA-toCUA+, CUA+toCUA+ CUtoMCI/AD,
74 MCItoMCI, MCItoAD, and ADtoAD. Subjects for which clinical diagnosis was not
75 available were excluded from the diagnostic group analysis. The associations with
76 diagnostic change groups were assessed by *post-hoc* Dunn's multiple comparison test
77 after non-parametric Kruskal-Wallis tests. Analysis was performed using Matlab (version
78 9.4) and GraphPad Prism (version 9.0.0).
79

Supplementary Figures

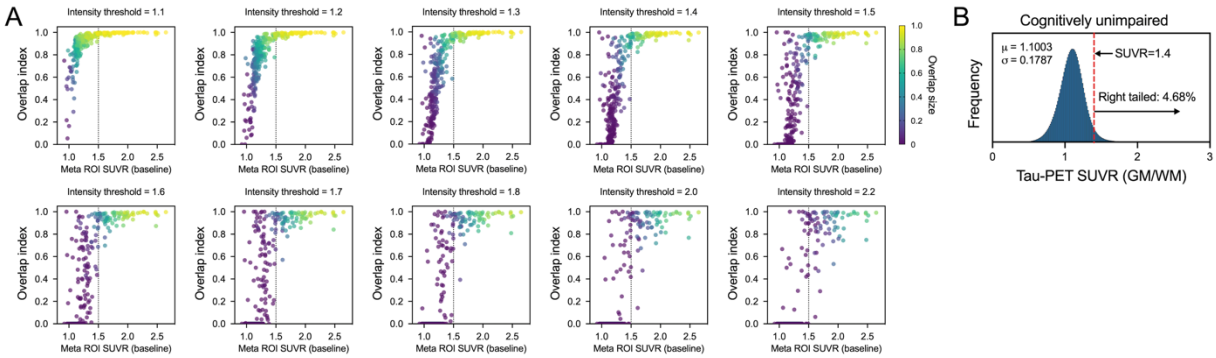

Supplementary Figure1. Intensity threshold comparison. (A) In order to determine the intensity threshold, experimental tests were performed for various threshold levels (from 1.1 to 2.2). We found that OI was easily saturated if the OI threshold was low because too many voxels were included in the mask. In contrast, if a more stringent threshold was applied, fewer voxels survived and the OI calculation became unstable. For these higher intensity thresholds, identifying abnormal regions is not typically a diagnostic dilemma and standard ROI analysis is sufficient. The threshold level used for the main analysis (SUVR=1.4) was determined observationally. (B) A histogram of voxel-wise SUVR values for all the gray and white matter in the brain over a cognitively unimpaired group was derived. The arbitrarily determined threshold (SUVR=1.4) corresponds to a right-tailed 4.68% (1.67xSD) meaning that the voxels with SUVR >1.4 are fairly rare in the brain of CU participants, serving as a reasonable threshold for the purposes of OI calculation.

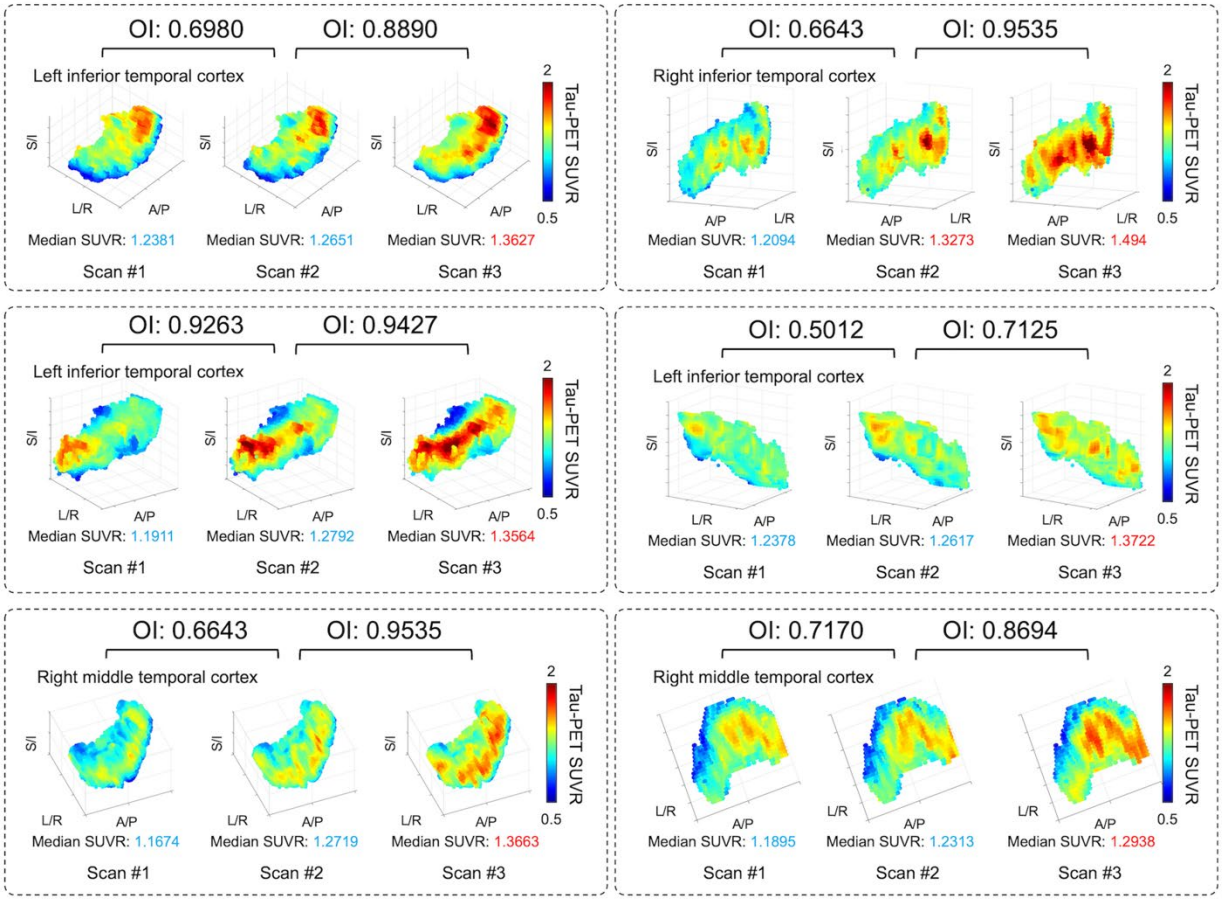

Supplementary Figure 2. Examples of high-OI cases. Three consecutive 3D scatter plots in each dotted box represent tau-PET SUVR of each voxel in each scan from an individual subject with high OI (>0.5) and low median SUVR at the first scan (<1.29).

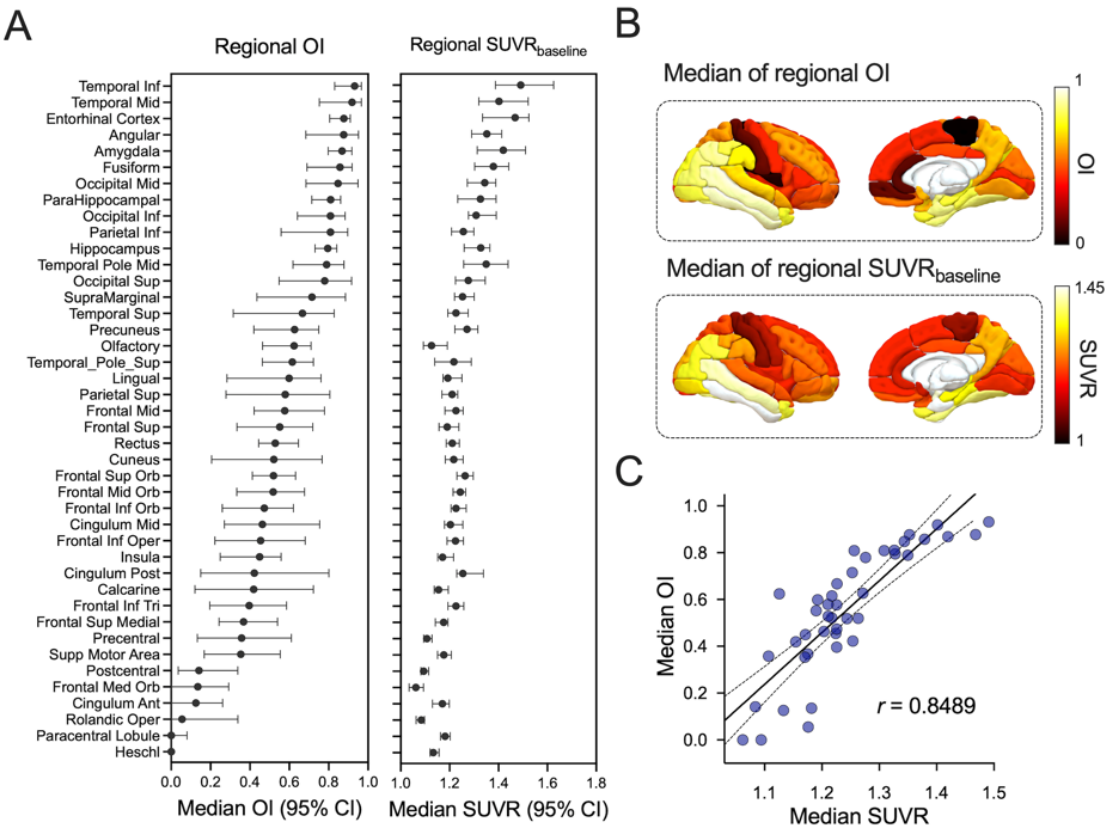

Supplementary Figure3. Topographical pattern of overlap index. (A) For each specific brain region, the median of regional OI and regional SUVR from CI cohort was displayed with 95% confidence intervals. The brain regions were sorted high to low in the median of regional OI. Bilateral hemispheres were used together for OI and SUVR calculation. (B) Median of regional OI and SUVR illustrated in 3D rendering plot. (C) The scatter plot illustrates an association between median SUVR and median OI. *r* indicates the Pearson's correlation coefficient. The black solid line and dotted lines represent a regression line and its 95% confidence band, respectively.

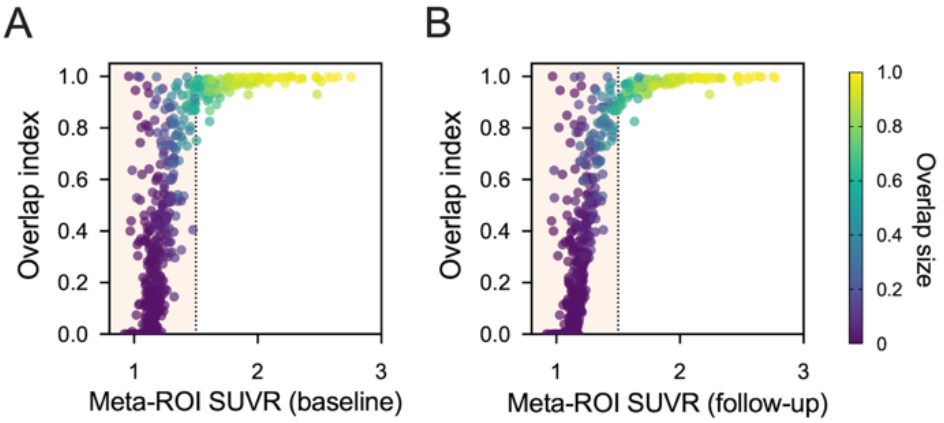

114 **Supplementary Figure 4. Association of OI with baseline and follow-up SUVR.** (A)
115 The scatterplot illustrates the association between baseline SUVR and OI for meta-ROI.
116 The dot's color indicates the overlap size. (B) The scatterplot illustrates the association
117 between follow-up SUVR and OI from meta-ROI. The dot's color indicates the overlap
118 size.
119

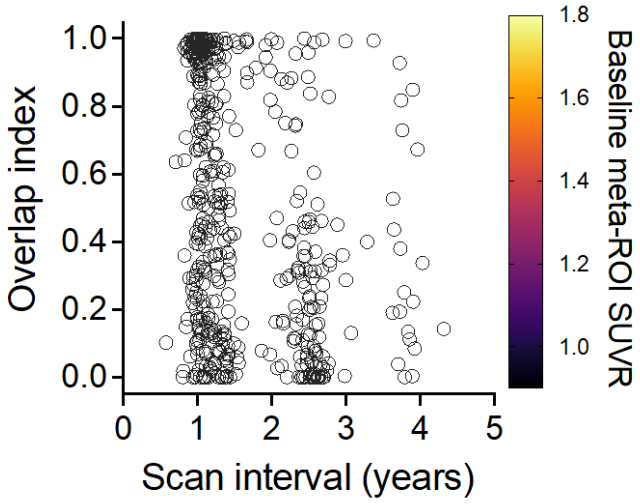

121 **Supplementary Figure 5. Association of OI with inter-scan interval.**

122

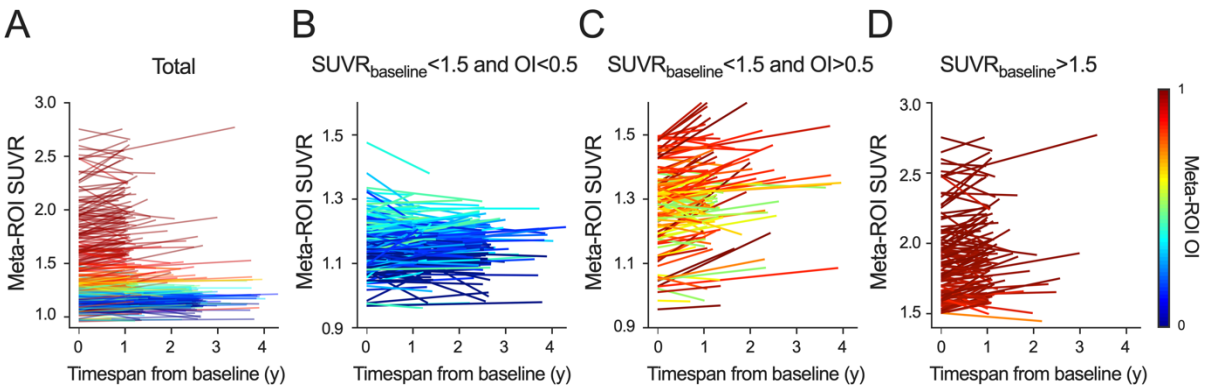

Supplementary Figure 6. (A) Spaghetti plot of SUVR trajectory from baseline to next follow-up showing meta-ROI SUVR for all individuals. The line color was coded by each individual OI. (B) Spaghetti plot of SUVR trajectory showing meta-ROI SUVR for SUVR<1.5 and OI<0.5. (C) Spaghetti plot of SUVR trajectory showing meta-ROI SUVR for SUVR<1.5 and OI>0.5. (D) Spaghetti plot of SUVR trajectory showing meta-ROI SUVR for SUVR>1.5.

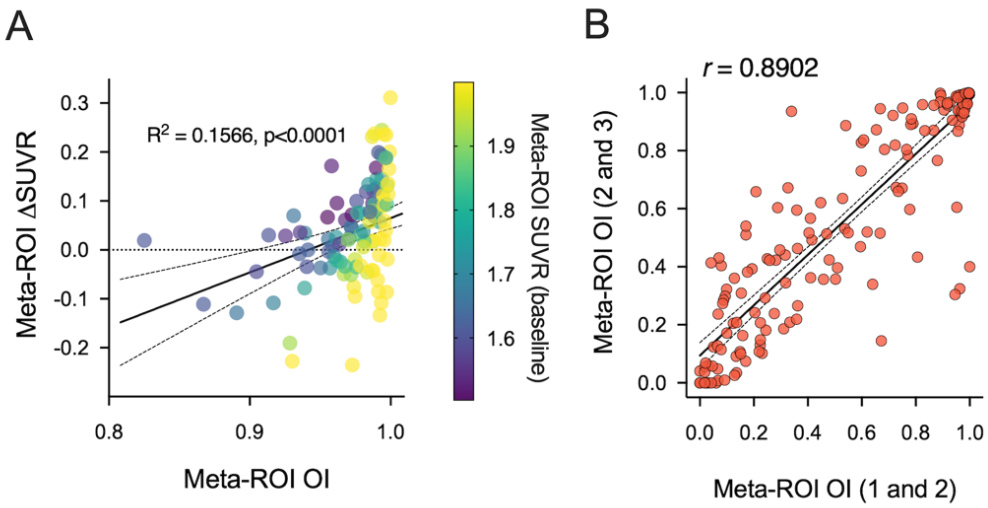

Supplementary Figure 7. (A) Association between meta-ROI OI and meta-ROI ΔSUVR where baseline SUVR>1.5. The black solid line and dotted lines represent a regression line and its 95% confidence band, respectively. (B) Consistency of the OI metric. The meta-ROI OI from the first and second scans and that from the second and third scans in the cohort who had three or more time points were compared. r indicates the Pearson's correlation coefficient.

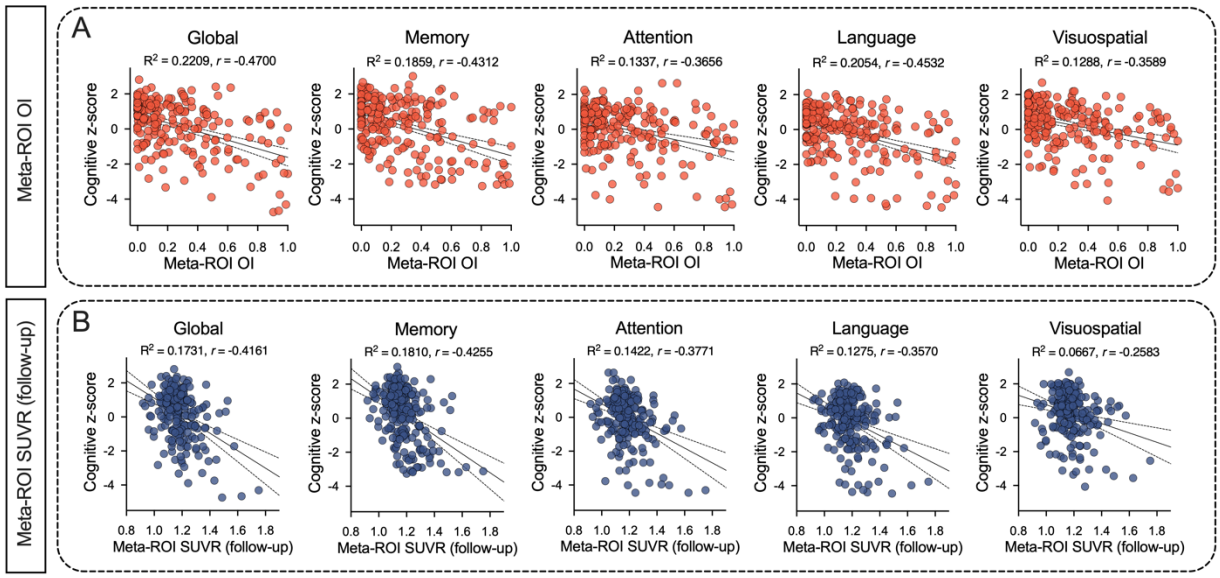

Supplementary Figure 8. Association of overlap index with cognitive scores. Four cognitive domains (memory, attention, language and visuospatial) and global scores (average of all domains) were tested. Only participants who had cognitive scores were included in this analysis (Supplementary Table1). (A) Relationship between meta-ROI OI and cognitive scores. The black solid line and dotted lines represent a regression line and its 95% confidence interval, respectively. r shows Pearson's correlation coefficient. (B) Relationship between meta-ROI ΔSUVR and cognitive scores. The black solid line and dotted lines represent a regression line and its 95% confidence interval, respectively. r shows Pearson's correlation coefficient.

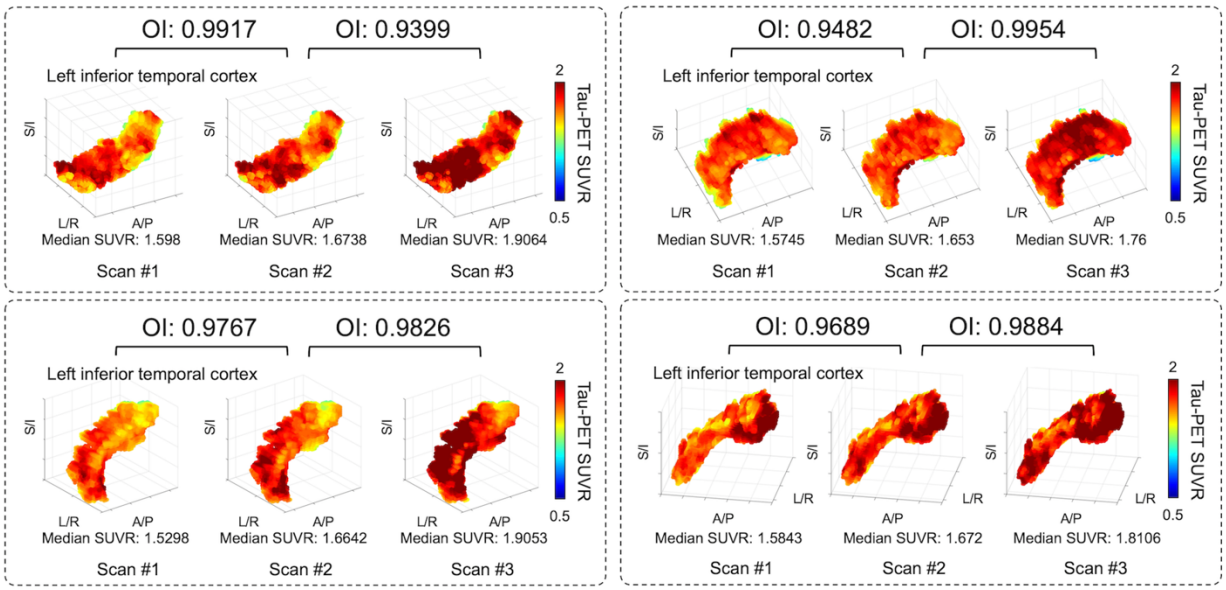

Supplementary Figure 9. Examples of high SUVR cases. Three consecutive 3D scatter plots in each dotted box represent the tau-PET SUVR of each voxel in each scan from an individual subject. OI becomes saturated (close to 1) in the high SUVR range because serial scans with abundant tau signals tend to be consistent.

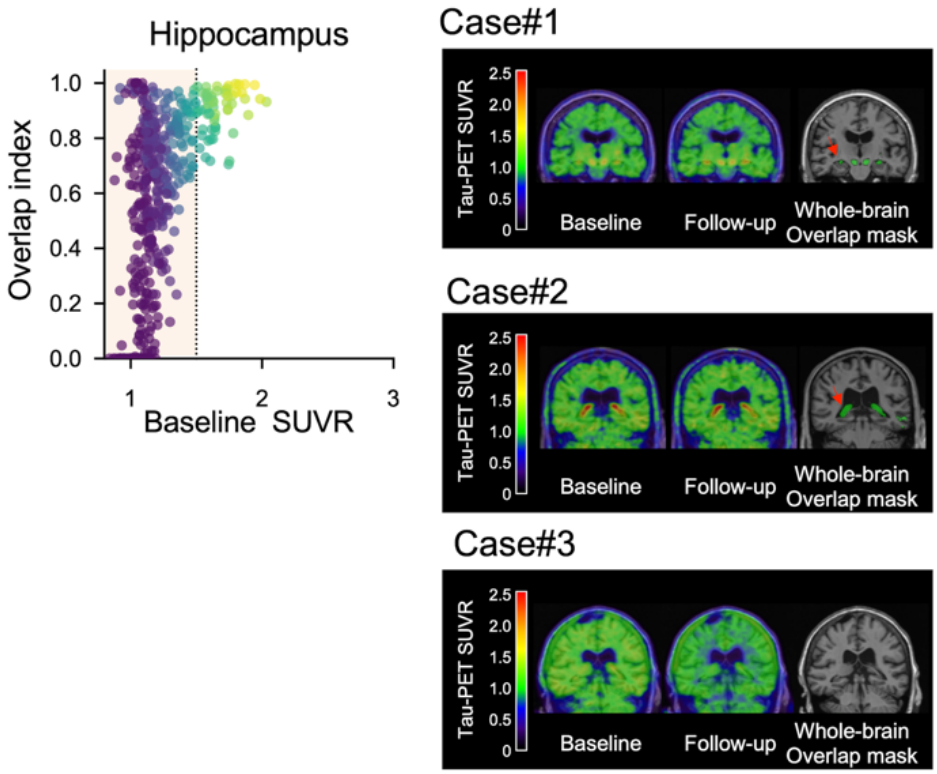

Supplementary Figure 10. Choroid plexus bindings. High OI was frequently observed in the lower baseline SUVR range in hippocampus. The coronal slices show the baseline tau-PET, follow-up tau-PET, and their overlap mask between high-intensity voxels (SUVR>1.4) for three representative cases. The red arrows indicate the choroid plexus overlap between baseline and follow-up scans.

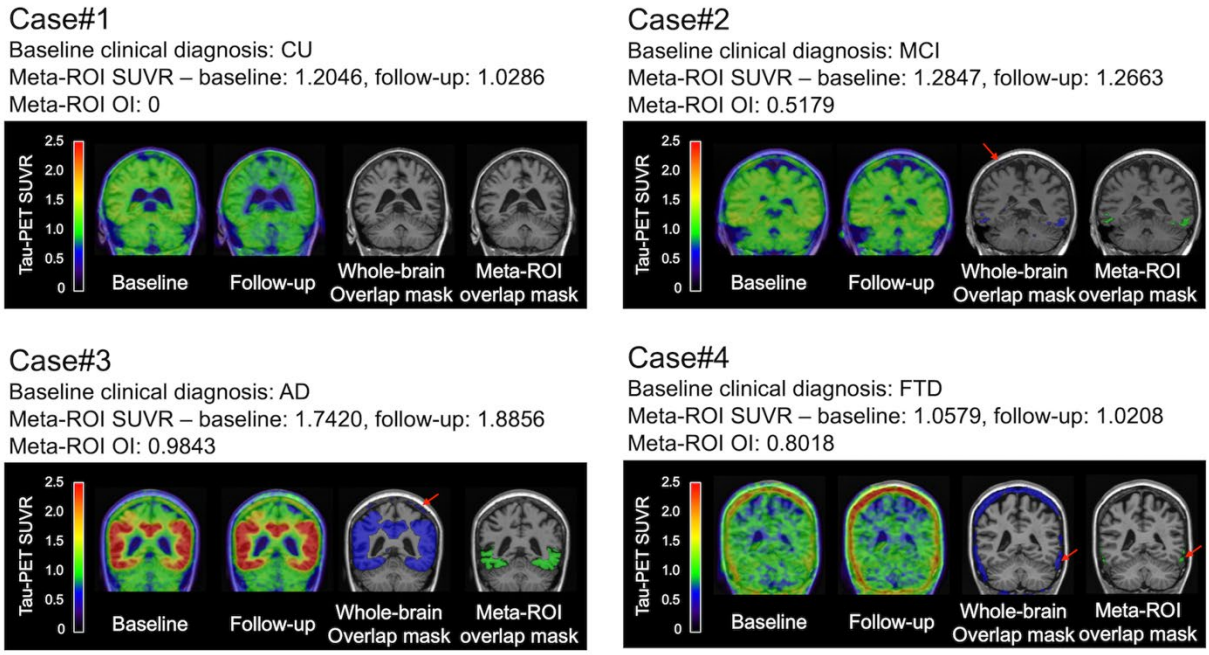

Supplementary Figure 11. Meninges binding. The coronal slices show the baseline tau-PET, follow-up tau-PET, overlap mask of whole brain and overlap mask within the meta-ROI for four representative cases. The red arrows indicate the meninges overlap between baseline and follow-up scans.

173 **Supplementary Table 1. Participant demographics.**

Baseline Characteristics	Summary
Number of participants (total)	339
Total tau-PET scans, n (%)	
2	189 (55.75)
3	129 (38.05)
>4	21 (6.19)
Time between consecutive scan, years*	
Median (IQR)	1.24 (1.04, 2.32)
Min, max	0.58, 4.32
Age at baseline PET, years	
Median (IQR)	68 (62, 76)
Min, max	33 95
Education, years {1}	
Mean (SD)	15.39 (2.66)
Male sex, n (%)	195 (57.52%)
PiB SUVR at baseline {16}	
Median (IQR)	1.72 (1.34 2.14)
Min, max	1.16 3.38
Diagnosis at baseline, n (%) {1}	
Cognitively Unimpaired	172 (50.74)
Mild Cognitive Impairment	62 (18.29)
Alzheimer's Dementia	47 (13.86)
Lewy Body Dementia	9 (2.65)
REM sleep Behavior Disorder	7 (2.06)
Frontotemporal Dementia	9 (2.65)
Posterior Cortical Atrophy	8 (2.36)
Logopenic Progressive Aphasia	2 (0.59)
Progressive Supranuclear Palsy	1 (0.29)
Progressive Fluent Aphasia/semantic aphasia	4 (1.18)
Progressive associative agnosia/prosopagnosia	1 (0.29)
Unknown	17 (5.01)
APOE ε4 carrier, n (%) {3}	128 (38.10)
Short Test of Mental Status score at baseline, median (IQR) {15}	35 (31 37)
Cognitive z scores at baseline, median (IQR)	
Global {174}	0.6906 (-0.3220 1.1513)
Memory {159}	0.6084 (-0.4529 1.3066)
Attention {165}	0.3680 (-0.4391 0.9368)
Language {159}	0.3230 (-0.4653 0.8395)
Visuospatial {170}	0.5789 (-0.0615 1.2111)

174 * Based on all scans for all individuals.

175 {} Brackets in the characteristics column indicate the number of participants missing this
176 particular variable.

177 **Supplementary Table 2. ADNI participant demographics.**

Baseline Characteristics	Summary
Number of participants (total)	235
Total tau-PET scans, n (%)	
2	158 (67.23)
3	67 (28.51)
>4	10 (4.26)
Time between consecutive scan, years*	
Median (IQR)	1.03 (0.98, 1.25)
Min, max	0.58, 2.92
Age at baseline PET, years	
Median (IQR)	74 (69, 79)
Min, max	56 90
Education, years	
Mean (SD)	16.32 (2.51)
Male sex, n (%)	112 (47.66%)
AV45 SUVR at baseline {75}	
Median (IQR)	1.17 (1.03 1.36)
Min, max	0.81 1.72
Diagnosis at baseline, n (%) {1}	
Cognitively Unimpaired	127 (54.04)
Mild Cognitive Impairment	78 (33.19)
Alzheimer's Dementia	30 (12.77)
APOE ε4 carrier, n (%) {6}	128 (48.47)

178

179 * Based on all scans for all individuals.

180 {} Brackets in the characteristics column indicate the number of participants missing this

181 particular variable.

Supplementary Table 3. Image IDs for ADNI cohort.

MRI_ImageID											
I573620	I1084935	I655397	I1142379	I990073	I1325694	I758062	I1316836	I640943	I1039209	I1185266	I1004681
I906797	I1266356	I910675	I1184047	I1153132	I1019265	I1068952	I1006005	I801187	I1222562	I1325980	I1182315
I1050345	I695035	I655561	I895057	I1086094	I1188738	I1047958	I1190195	I955110	I766317	I1012942	I996464
I687384	I916119	I920960	I1142367	I1253141	I1326332	I1229050	I1325533	I1116518	I992457	I1320847	I1169375
I848000	I1060804	I594111	I1264767	I1136371	I1037228	I1189749	I1091694	I1276857	I852333	I1021751	I1045984
I1001975	I1244529	I883929	I1223029	I1267719	I1219059	I1116451	I1286418	I515359	I985405	I1195531	I1227239
I774046	I905391	I909607	I1342083	I879552	I927354	I1263792	I956599	I775626	I1154866	I1328524	I1046736
I854584	I1060894	I1044187	I987370	I1196891	I1117449	I901163	I1119606	I903950	I832079	I1023583	I1226810
I1010814	I1228309	I1225879	I1158135	I881980	I916492	I1042399	I1278852	I1081537	I974779	I1215774	
I884806	I937847	I767926	I929044	I1025881	I1116728	I1215232	I984878	I520149	I1020096	I1329845	
I1042944	I1081546	I902899	I1135165	I1225896	I957103	I729610	I1221363	I914038	I1185714	I1049755	
I835740	I974757	I860224	I1251421	I666359	I1165397	I858531	I1050518	I781037	I1069951	I1245803	
I988538	I1157071	I1011352	I956815	I944327	I991861	I1010150	I1236425	I905324	I1260118	I507327	
I1270100	I876555	I569607	I1275051	I849901	I1211451	I1173416	I925543	I794165	I1186906	I1056754	
I912447	I1025741	I854572	I947480	I996840	I728268	I898538	I1214021	I922614	I1326101	I1225162	
I1235535	I1186516	I748885	I1264016	I1174915	I1117314	I1040539	I909791	I674977	I841950	I858503	
I973293	I940882	I876699	I714589	I1061844	I1293452	I1251515	I1116890	I882274	I1162407	I1161837	
I1160987	I1132797	I1020355	I942773	I1259263	I527063	I1014602		I727179	I530861	I839474	
I1001084	I985197	I1020137	I1263811	I1058589	I818409	I1215046	I1257600	I859212	I784788	I1170878	
I1185102	I1160021	I1195772	I1003363	I1253903	I599501	I1038250	I879209	I890738	I549854	I887923	
I1005735	I998447	I1327210	I1175340	I919238	I824980	I1278681	I1092240	I1042463	I796487	I1116406	
I1227039	I1170118	I1092176	I1003993	I1058029	I709524	I908698	I980928	I1219049	I573499	I1229457	
I1005884	I1041482	I1282405	I1186737	I955473	I914845	I1303143	I1226508	I521553	I799802	I935952	
I1196215	I1193331	I1177672	I1030818	I1117701	I952046	I892784	I977141	I871944	I911048	I1264670	
I1012896	I902070	I1328418	I1227943	I1285188	I1146201	I1238877	I1123765	I1018794	I1230243	I961814	
I1205679	I1079424	I935824	I1114881	I957065	I973541	I874427	I1304066	I1184723	I634514	I1136571	
I1016012	I1267860	I1274808	I1296792	I1281495	I1214910	I1033744	I1092329	I508766	I861323	I1299107	
I1190913	I784921	I946297	I975780	I938292	I971779	I1233982	I1120772	I893677	I638471	I874879	
I905360	I914397	I1086072	I1170596	I1072872	I1190623	I963756	I1281547	I1053655	I858986	I1252024	
I1058014	I1225000	I1241872	I880427	I1258040	I1003961	I1167981	I945601	I931614	I1004652	I892759	
I1236721	I908586	I958011	I1079905	I942819	I1223550	I974164	I1122101	I1263330	I1169363	I1256135	
I963926	I1067189	I1117156	I1179769	I1070545	I1017725	I1175747	I1281566	I1003918	I663669	I900796	
I1133565	I1239410	I1278640	I904007	I1250808	I1196850	I947589	I1017005	I1226896	I878250	I1284408	
I965825	I899473	I1029584	I1067140	I984807	I644636	I1182766	I1181047	I1331291	I705049	I946980	
I1149858	I1072377	I1224869	I1224698	I1165491	I915902	I1004663	I1038941	I1003831	I863101	I1167318	
I969773		I874250	I634541	I996786	I654979	I1179083	I1261558	I1180976	I703846	I1299334	
I1248433	I907713	I1029492	I814950	I1174125	I914178	I699539	I1226101	I1029798	I862838	I882167	
I978374	I1072841	I864643	I774420	I1084921	I641037	I943600		I1226436	I1017893	I1040207	
I1158785	I1254369	I1023178	I847364	I1175032	I931962	I1293823	I1053608	I1021434	I1180387	I1063917	
I989656	I1037958	I1184858	I582706	I1045204	I884453	I1040222	I1280955	I1199335	I928920	I1258251	
I1170103	I1241180	I879343	I814318	I1233828	I1046066	I1264179	I1003342	I1042262	I1071232	I1019281	
I1020186	I1023727	I1030385	I845672	I769864	I1213040	I1066557	I1165186	I1233686	I1257943	I1237279	
I1214052	I1282313	I1189912	I1091790	I919448	I971712	I1269091	I1027771	I1073644	I931630	I923853	
I925944	I820302	I1274391	I1285558	I1053099	I1195542	I859714	I1207638	I1243100	I1073317	I1075536	
I1064236	I1173060	I1155909	I508493	I1241095	I1287821	I1212969	I1040533	I741448	I1256452	I763562	
I1244513	I820315	I848162	I941140	I817507	I881729	I905866	I1226120	I1221690	I991768	I893552	
I902659	I1172863	I1173479	I872012	I959742	I1033364	I1071981	I1129344	I1194945	I1164436	I1037531	
I1060837	I905773	I831854	I1190570	I1278606	I1185877	I1276990	I1293353	I1023753	I1000359	I1225971	
I695091	I1043303	I1152869	I1133905	I1017993	I1008726	I976382	I901027	I1273042	I1177292	I1170562	
I942907	I1227288	I844181	I1149150	I1194953	I1177833	I1189640	I1234305	I744805	I1003730	I1333802	

AV1451_ImageID											
I632551	I1111061	I678812	I1158520	I996426	I1325693	I759978	I1320231	I735701	I1044233	I1185100	I1002757
I915198	I1264643	I922853	I1175890	I1153594	I1037696	I1148714	I1014100	I813346	I1221440	I1325727	I1193061
I1054822	I761277	I678811	I901602	I1084423	I1196051	I1055279	I1221773	I1001616	I762011	I1020495	I1007447
I689622	I918783	I927331	I1142357	I1242137	I1326425	I1233685	I1327166	I1117126	I1001314	I1320670	I1170613
I848039	I1062327	I678791	I1320862	I1075017	I1041479	I968220	I1122345	I1281760	I855614	I1033172	I1064703
I1001342	I1245623	I886311	I1234740	I1253056	I1226872	I1116637	I1290882	I555842	I985481	I1195667	I1229517
I761550	I906514	I912364	I1343146	I877000	I929659	I1261995	I982149	I776104	I1155676	I1328673	I1065699
I854548	I1057549	I1050819	I989161	I1227883	I1117483	I890306	I1122087	I912510	I834601	I1043063	I1237135
I1010905	I1229125	I1227296	I1157437	I882211	I948378	I1044156	I1288929	I1083089	I976392	I1217092	
I886723	I944916	I779832	I929657	I1033141	I1116815	I1204900	I989766	I568490	I1027264	I1330199	
I1052023	I1082590	I894432	I1136606	I1223547	I998996	I757685	I1221516	I916462	I1185997	I1073021	
I844301	I981120	I861627	I1294031	I716777	I1175420	I871078	I1057528	I781192	I1111058	I1245999	
I989358	I1158521	I1009363	I952961	I948931	I1012521	I1012785	I1236646	I909074	I1262816	I529864	
I1168115	I879716	I645864	I1290919	I855396	I1215414	I1171597	I939926	I797939	I1191369	I1046083	
I973677	I1049759	I854890	I948017	I1002174	I757443	I899021	I1231670	I935224	I1327165	I1228651	
I1262171	I1187407	I759181	I1262400	I1171298	I839801	I1038465	I957413	I685059	I860730	I873235	
I992116	I943320	I875798	I722171	I1073404	I1173455	I1236776	I1116816	I925730	I1163599	I1160604	
I1161478	I1137473	I1027199	I943715	I1258425	I535759	I1035169	I1035292	I762010	I531824	I857653	
I1028655	I994488	I1026299	I1265227	I1072607	I828552	I1213428	I1262032	I869273	I784842	I1167658	
I1187329	I1169561	I1195806	I1024097	I1269070	I609338	I1059605	I916758	I901721	I555841	I900852	
I1082828	I1005530	I1325985	I1185074	I920023	I832340	I1277166	I1086512	I1054761	I796600	I1133156	
I1232169	I1181217	I1122765	I1043849	I1058323	I655452	I916106	I1035872	I1221299	I575577	I1234818	
I1039770	I1036653	I1278636	I1185615	I956633	I928843	I1318181	I1226547	I576868	I801328	I941809	
I1196168	I1193569	I1181493	I1057990	I1117942	I980567	I916364	I1014852	I873894	I907301	I1280072	
I1047876	I916842	I1329807	I1227973	I1285731	I1146464	I1256924	I1120276	I1054762	I1230069	I968770	
I1208729	I1079439	I974428	I1137145	I961041	I1012934	I916934	I1309539	I1199224	I635350	I1135903	
I1028622	I1267876	I1291668	I1299208	I1282375	I1214947	I1045199	I971992	I576858	I861365	I1335357	
I1191956	I729585	I973368	I979051	I943092	I991914	I1266271	I1118166	I894156	I640890	I921073	
I915150	I1041349	I1139353	I1177259	I1074913	I1191054	I964166	I1282058	I1054764	I860689	I1265214	
I1084509	I1234239	I1296765	I880519	I1258422	I1029875	I1167991	I967179	I940476	I1005528	I948327	
I1253775	I952534	I985145	I1014149	I943916	I1223593	I979045	I1122296	I1263013	I1169969	I1289208	
I966777	I1067557	I1122007	I1185747	I1070905	I1037778	I1175531	I1282205	I1037548	I665386	I959272	
I1156624	I1245622	I1280781	I902477	I1252409	I1196938	I947218	I1039309	I1204356	I879650	I1304876	
I980183	I931634	I1046001	I1069666	I1002243	I661476	I1212957	I1181068	I1331674	I703850	I954228	
I1178524	I1083272	I1260274	I1225478	I1166025	I914338	I1005345	I1051418	I1010745	I863145	I1173776	
I989600	I1236749	I874246	I634595	I1011867	I688379	I1226870	I1212547	I1232682	I705442	I1299329	
I1215678	I933778	I1034882	I825213	I1174530	I914307	I758437	I1224187	I1044452	I862881	I948324	
I994547	I1086582	I865025	I609005	I1027052	I715595	I945858	I1332635	I1226633	I1021608	I1041516	
I1176101	I1254558	I1023510	I850410	I1174569	I931886	I1277704	I1059052	I1033420	I1175287	I1073650	
I999959	I1059394	I1185226	I583146	I1051880	I888176	I1063933	I1186099	I1201288	I932177	I1259707	
I1186600	I1241791	I879177	I822292	I1233915	I1045791	I1230328	I1012933	I1117705	I1071356	I1053661	
I1047950	I1053983	I1043841	I872314	I767719	I1214694	I1133949	I1166024	I1233963	I1258171	I1238936	
I1226631	I1278088	I1190145	I1093847	I916329	I963437	I1265504	I1029868	I1070544	I939115	I961494	
I939955	I820839	I845498	I1290884	I1079242	I1158513	I895899	I1231589	I1243166	I1073656	I1131610	
I1070646	I1173496	I1158935	I522567	I1246034	I1276863	I1214758	I1056586	I758381	I1256652	I770868	
I1241113	I820887	I850020	I941743	I817759	I876966	I940749	I1239548	I1048080	I994529	I892783	
I902928	I1173497	I1175896	I959495	I977640	I1022152	I1073622	I1137574	I1188951	I1173979	I1050688	
I1048797	I908216	I837132	I1222949	I1282723	I1185959	I1279368	I1299304	I1083271	I1006574	I1240834	
I758085	I1048815	I1184059	I971747	I1040305	I1048282	I984226	I920752	I1185528	I1177663	I1168259	
I946089	I1232727	I858115	I1145242	I1206710	I1178741	I1191368	I1232729	I761087	I1017333	I1333863	

Supplementary Table 4. Multivariate regression analysis. Each independent variable was standardized (i.e., centering and scaling) for the analysis.

Variables	Coefficient (95% Confidence interval)	P value
Scan interval	-0.04512 (-0.06856 to -0.02168)	0.0002
Baseline SUVR	0.2506 (0.2271 to 0.2740)	<0.0001
Intercept	0.4881 (0.4657 to 0.5105)	<0.0001

REFERENCES

1. Joshi A, Koeppe RA, Fessler JA. Reducing between scanner differences in multi-center PET studies. *Neuroimage.* 2009;46:154-159.

2. Schwarz CG, Wiste HJ, Gunter JL, et al. Variability in MRI and PET measurements introduced by change in MRI vendor. *Alzheimers Dement.* 2019;15:P104-P105.

3. Tzourio-Mazoyer N, Landeau B, Papathanassiou D, et al. Automated anatomical labeling of activations in SPM using a macroscopic anatomical parcellation of the MNI MRI single-subject brain. *Neuroimage.* 2002;15:273-289.

4. Vemuri P, Whitwell JL, Kantarci K, et al. Antemortem MRI based STructural Abnormality iNDex (STAND)-scores correlate with postmortem Braak neurofibrillary tangle stage. *Neuroimage.* 2008;42:559-567.

5. Ashburner J, Friston KJ. Unified segmentation. *Neuroimage.* 2005;26:839-851.

6. Vemuri P, Senjem ML, Gunter JL, et al. Accelerated vs. unaccelerated serial MRI based TBM-SyN measurements for clinical trials in Alzheimer's disease. *Neuroimage.* 2015;113:61-69.

7. Lowe VJ, Lundt ES, Albertson SM, et al. Tau-positron emission tomography correlates with neuropathology findings. *Alzheimer's & Dementia.* 2019.

8. Jack Jr CR, Wiste HJ, Schwarz CG, et al. Longitudinal tau PET in ageing and Alzheimer’s disease. *Brain.* 2018;141:1517-1528.

9. Jack Jr CR, Wiste HJ, Weigand SD, et al. Defining imaging biomarker cut points for brain aging and Alzheimer's disease. *Alzheimers Dement.* 2017;13:205-216.

10. Meltzer CC, Leal JP, Mayberg HS, Wagner Jr HN, Frost JJ. Correction of PET data for partial volume effects in human cerebral cortex by MR imaging. *J Comput Assist Tomogr.* 1990;14:561-570.